Physica D 443 (2023) 133587

Contents lists available at ScienceDirect

Physica D

journal homepage: www.elsevier.com/locate/physd

Switching between periodic orbits in impact oscillator by time-delayed feedback methods

Dimitri Costa [a,b,*], Vahid Vaziri [a], Ekaterina Pavlovskaia [a], Marcelo A. Savi [b], Marian Wiercigroch [a]

[a] Centre for Applied Dynamics Research, School of Engineering, University of Aberdeen, King's College, Scotland, Aberdeen AB24 3FX, United Kingdom
[b] Center for Nonlinear Mechanics, COPPE - Department of Mechanical Engineering, Universidade Federal do Rio de Janeiro, 21.941.972 Rio de Janeiro - RJ, P.O. Box 68.503, Brazil

ARTICLE INFO

Article history:
Received 17 March 2022
Received in revised form 16 September 2022
Accepted 1 November 2022
Available online 11 November 2022
Communicated by Dmitry Pelinovsky

Keywords:
Nonsmooth dynamics
Nonlinear control
Multi-stability
Delayed systems

ABSTRACT

An ability to exchange between different attractors can bring adaptability and new functionalities to an engineering system. While nonlinear controllers are widely used to stabilize on a preferred orbit, there is only a few which can exchange back and forth between two or more stable periodic responses. This work proposes a new variation of the original Time-Delayed Feedback (TDF) control method capable to effectively switch back and forth between periodic orbits having only a limited knowledge of the system dynamics. The stable or unstable periodic responses of the system that are inside or outside a chaotic attractor can be targeted. The proposed control method named here as the Fractional Time-Delayed Feedback Control (FTDF) is tested numerically and experimentally using a newly developed impact oscillator rig. Various responses including impacting and non-impacting orbits, high period attractors and chaos are considered. The main advantages of the FTDF over the TDF are presented by showcase scenarios where the TDF alone cannot safely perform the exchange between orbits.

1. Introduction

The idea of adaptable systems has been widely applied to various fields in engineering, ranging from origami structures [1,2] that use folds to change their configuration, to energy harvesters [3] that require a wide spectrum of dynamical behaviour depending on external excitation. This adaptability can be explored by a modification of the system parameters or by utilizing the phenomenon of multi-stability where, depending on the initial conditions, qualitatively and quantitatively different persisting dynamical responses known as co-existing attractors are present.

Multi-stability is an inherent fabric of many strongly nonlinear dynamical systems, and manifests itself widely in science and engineering. For example, in impact oscillators, multi-stability is a common phenomenon [4,5]. Multi-stability can also be found on microelectromechanical devices (MEMS) [6], in drill string dynamics [7], among others. In the case of impact systems, multi-stability between impacting and non-impacting attractors has a crucial role in the system operation. Depending on the application, impacts can be the desired behaviour as in the Resonance Enhanced Drilling [8–10], seismic mitigation [11], and energy harvesters [12] or an undesired one that should be avoided to prevent damages and imperfections as in machining [13,14]. In all cases, the ability to choose the system response between impacting and non-impacting co-existing attractors can be a crucial part of the system operation [15].

In investigations of multi-stable systems, the piecewise linear impact oscillators are extensively studied as simple models that present such phenomena [4] and can be used to model various applications in engineering. A significant contribution to this area has been made by the Centre for Applied Dynamics Research (CADR) at the University of Aberdeen often inspired by applications including a new drilling method [16] and supported by fundamental studies involving experimentally calibrated models like a piecewise linear impact oscillator exhibiting co-existing solutions with chaotic and periodic co-existing attractors including impacting and non-impacting orbits, among others [17–20]. Recently, a new direct mass excited impact oscillator capable of high accuracy experiments has been developed and tested by the CADR [21,22], which exhibits naturally multi-stability and can be a platform for implementing and testing new control methods.

In contrary to the classical control methods where potential advantages of the natural system dynamics are rarely exploited, the general idea of chaos control, is to stabilize a dynamical system by small perturbations on one of its desired but unstable

* Corresponding author at: Centre for Applied Dynamics Research, School of Engineering, University of Aberdeen, King's College, Scotland, Aberdeen AB24 3FX, United Kingdom.
E-mail address: dimitri.costa@abdn.ac.uk (D. Costa).

https://doi.org/10.1016/j.physd.2022.133587

periodic orbits as proposed in discrete [23] and continuous [24] chaos controllers. In the field of continuous control, various authors have based their studies on the TDF [24]. Sacollar et al. [25] proposed one main modification by introducing the influence of multiple delayed states into the control signal. Other works modified the TDF itself to require less information about the controlled system by automatically tuning its parameters such as the proportional gain [26,27] or the time-delay [28]. Some studies even reshaped the TDF to overcome the limitations identified in [29] to stabilize orbits that have an odd number of positive Floquet exponents by introducing so-called periodic gains [30,31] or additional unstable states [32]. Pyragas and Pyragas [33–35] proposed modifications of the TDF method to avoid the introduction of an infinite number of Floquet multipliers which facilitates the optimization and design of the controllers, whist Jüngling et al. [36] explored the use of variable delays for the TDF control. De Paula et al. [37] applied the TDF method to control experimentally bifurcations of a parametric pendulum, while Costa et al. [38] used the same strategy in an SMA two-bar truss. Other notable works on the TDF method include modelling of frictional systems [39,40] and control of cardiac rhythms [41]. Angelo et al. [42] applied the TDF method to an atomic force microscope and Höhne et al. [43] studied properties of the time-delayed feedback controller with an unstable control loop (UTDF) experimentally. Other works have utilized the TDF idea into fractional [44,45] and quantum [46,47] systems. Recently, Zhang et al. [48] analysed how the TDF control can affect the basins of co-existing attractors near grazing in a soft impacting system, suggesting that TDF can be used to control their co-existence.

Despite all these control efforts, the TDF control was never applied to switch between coexisting attractors. In fact, only a few significant works have been published on alternative control approaches for switching between attractors. One notable example is the work by the CADR [49] that proposes a controller to perform exchange between different attractors by temporarily eliminating the current evolution of the system and introducing the desired evolution using a linear control signal. After stabilization, the control signal also goes to zero as the introduced behaviour needs to be part of the system original attractors. Although this strategy can successfully exchange between two attractors, it requires the full knowledge of both responses, access to all the system state variables, and tracking of the excitation signal for non-autonomous systems. Recently, Zhi et al. [50] proposed a new control approach to switch between co-existing attractors, which needs to be further investigated.

This work proposes a new variant of the original Time-Delayed Feedback control based on the controller time delay that is able to switch between co-existing stable and unstable periodic orbits with a low knowledge requirement. TDF and this new method are tested experimentally and numerically on the newly developed impact oscillator [21,22] for few typical responses including impacting and non-impacting orbits, high period oscillations and chaos. Initially, the analysis of the system dynamics is performed and four scenarios are selected to assess the control strategy capabilities. In three scenarios, the TDF method can successfully switch between the selected co-existing attractors. However, in one scenario, the TDF cannot perform the exchange and the modification proposed in this work is required for a successful control.

The rest of the article is structured as follows. Section 2 presents the experimental apparatus, its numerical model and describes the system dynamics used to test the control methods. In Section 3 the TDF control and ways to analyse its properties through Floquet theory are discussed. Afterwards, the exchange between the co-existing attractors in four selected cases is discussed and explored both experimentally and numerically. Section 4 introduces the new FTDF and compares it to the TDF method in the last scenario where the TDF alone cannot perform the exchange between the co-existing attractors. Section 5 draws the main conclusions and provides some recommendations for future works.

2. Experimental impact oscillator and example responses

In this study, the newly developed impact oscillator described in [21,22] and modelled in [51] is used to investigate the applicability of TDF based control methods. Its schematics and photograph can be seen in Fig. 1(a), showing the oscillator mounted on a rigid structure. The oscillating mass is attached to the structure by two leaf springs which are clamped between grooved plates on each end. A strong neodymium magnet is also attached to the main mass by a stainless steel rod. The excitation is provided by the interaction between the magnet and an in-house built coil that can generate a varying magnetic field depending on the current I passing through it. This current is produced by a signal generator based on a National Instruments board and a in-house built amplifier constructed to produce a wide variety of excitation signals. The experimental data is collected by a LabView data acquisition system. The coil input current is sensed by a multimeter, while the displacement of the mass is measured by a eddy current probe attached to the rigid structure at the base of the leaf springs. Finally, there is a miniature force transducer placed between the rigid structure and the coil, that senses the reaction force due to the mass excitation. There are also accelerometers placed on the mass, rigid structure and impact beam.

A physical model of the experimental rig is shown in Fig. 1(b). The oscillator can be considered as a piecewise linear system, if the displacement, X, of the oscillating mass, m, is limited to an absolute displacement of 6 mm [22]. In the model, the force F_{coil} is applied directly to the main mass while the restoring force provided by the leaf springs is considered to be linear and characterized by the stiffness k_1. The impact beam is modelled as another linear spring with stiffness k_2, while a linear damping coefficient c is used to describe energy dissipations, leading to the equation of motion [22]:

$$\ddot{X} = -\frac{k_1}{m}X - \frac{k_2}{m}(X-g)H(X-g) - \frac{c}{m}\dot{X} + \frac{F_{coil}}{m}, \tag{1}$$

where $H(\cdot)$ is the Heaviside's step function and dot represents time derivative.

In this work, the mass displacement is considered to be the observable variable of the system and it is acquired with the eddy current probe. The sample rate for displacement is at least 200 times higher than the excitation frequency $f = \omega/2\pi$. The velocity is obtained by differentiating the filtered displacement signal using the symmetric difference quotient [52] with a frequency at least 10 times greater than f. Hence, the actuation frequency is also at least 10 times greater than f, and is set to ensure that the assumption of a continuous actuation is valid.

A calibration of the electromagnetic exciter was carried out in [22] to determine a relationship between the applied current and the generated force acting on the mass. The linear behaviour between the electromagnetic force and current was observed in the range of current amplitude up to 3.5 A and excitation frequencies up to 10 Hz. Hence, the coil can provide a force F_{coil} that is a sum of the harmonic excitation applied to the system $F_{exc} = aI_0 sin(\omega t)$, where I_0 is the excitation current amplitude and t is time, and actuation force $F_{act} = aI_{act}$ which is dictated by the control method.

The total force applied to the mass through the coil is then given by:

$$F_{coil} = F_{exc} + F_{act} = a(I_{exc} + I_{act}). \tag{2}$$

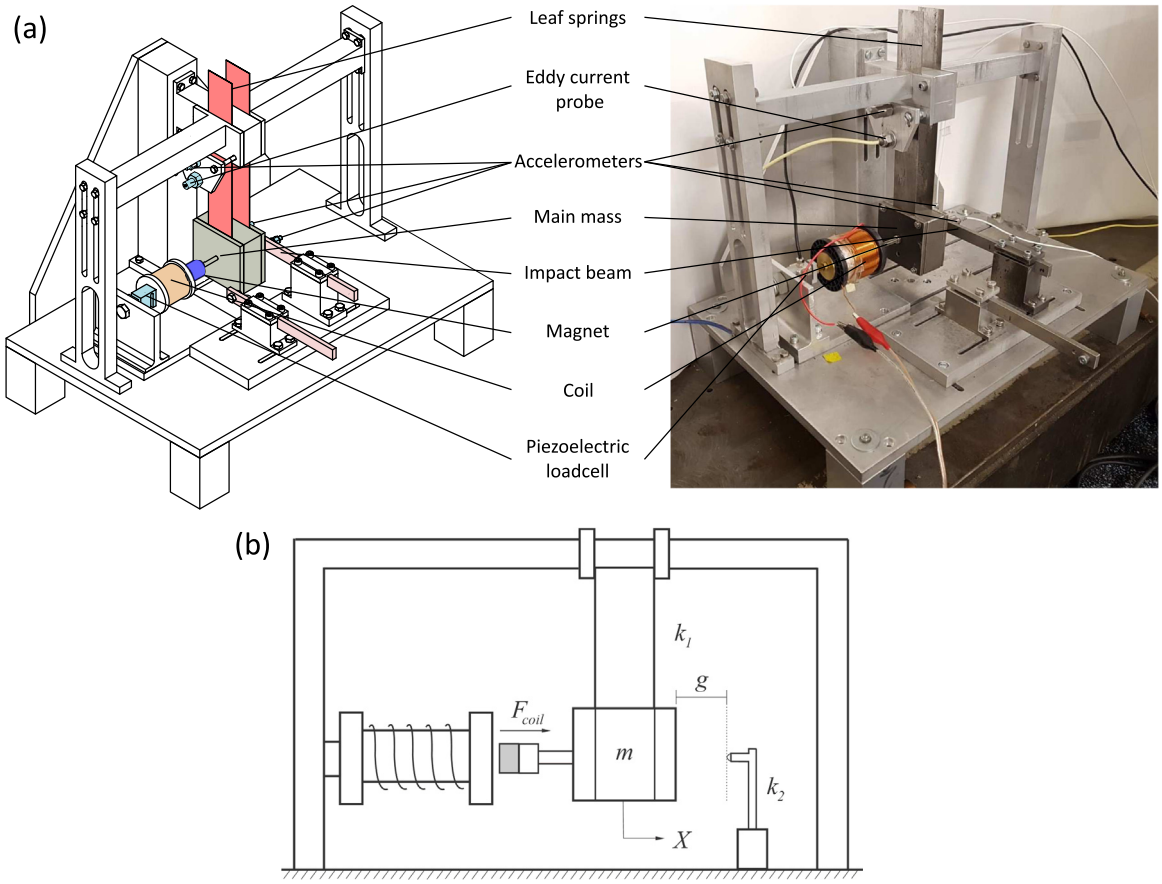

Fig. 1. Experimental impact oscillator developed in [21]; (a) 3D schematic diagram (left) and a photograph of the apparatus (right). The main components of the system are highlighted as: sensors (eddy current probe, piezoelectric load cell and accelerometers mounted on the mass, frame and impact beam) in light blue, coil in orange, main mass in grey, impact beams in pink, leaf springs in red and permanent magnet in dark blue [22]. (b) Schematics of physical model representing the experimental rig with its main components: main mass m, leaf springs of stiffness k_1, impact beam of stiffness k_2, coil generating force F_{coil} and the gap g between the main mass and the impact beam.

Table 1
Parameters values for the investigated piecewise linear model.

Symbol	Value	Unit
m	1.325	kg
k_1	4331	N/m
k_2	87 125	N/m
c	0.27	kg/s^2
g	0.74 10^{-3}	m
a	0.799	N/A
I_0	1.45	A

The complete system equations including actuation can be then given by:

$$\dot{\mathbf{x}} = \begin{bmatrix} \dot{X} \\ \ddot{X} \end{bmatrix} = \begin{bmatrix} \dot{X} \\ -\frac{k_1}{m}x - \frac{k_2}{m}(X-g)H(X-g) - \frac{c}{m}\dot{X} + \frac{a}{m}(I_{exc}+I_{act}) \end{bmatrix}, \quad (3)$$

Initially, the system dynamics is explored to identify the frequencies where co-existing attractors are present. The diagrams are constructed taking the last 100 periods and discarding the first 40 s of data for each quasi-static variation of frequency, which practically means that at least 240 periods are discarded as the transient response of the system. Experiments are performed for the set of identified parameters as listed in Table 1 and the results are presented in Fig. 2. The responses marked in black and blue are obtained when increasing frequency f and the red one when decreasing the frequency. It can be seen in Fig. 2(b), at lower frequencies up to 7.1 Hz, there is a co-existence between period-2 impacting and period-1 non-impacting orbits. Afterwards, a narrow window with only period-1 orbit is visible until a grazing incidence occurs at 7.15 Hz, which is followed by a typical chaotic-like behaviour [20,22]. Then we see a co-existence of a period-5 orbit with 3 impacts and a period-2 responses, shown in Fig. 2(c) up to 7.36 Hz. At this point, a grazing incidence occurs on the inner loops of the period-5 response causing the system to jump to another period-5 orbit with two impacts, which is depicted in Fig. 2(d). The co-existence of period-5 and period-2 lasts up to 7.50 Hz, where the period-5 orbit becomes unstable due to the grazing of one of its inner loops. At 7.78 Hz a period-doubling bifurcation cascade is observed leading to a chaotic response with its attractor shown in Fig. 2(e). The chaotic behaviour is maintained up to 8.28 Hz, where it gives way to a period-1 orbit. The four cases at frequencies $f = 6.8,\ 7.3,\ 7.4$ and 8.18 Hz, shown in Fig. 2(b) to (e), are selected to perform the exchange target control.

These cases are selected to test the control method chosen to exchange between co-existing attractors, and they are presented in Table 2. The case of $f = 8.18$ Hz, where the control stabilizes different unstable periodic orbits embedded in the chaotic attractor, is chosen to study the TDF control for the scenario which it was originally designed for. The two cases of period-2 and period-5 co-existing attractors scenarios at $f = 7.3$ and 7.4 Hz are chosen to evaluate how the TDF control performs. The last case

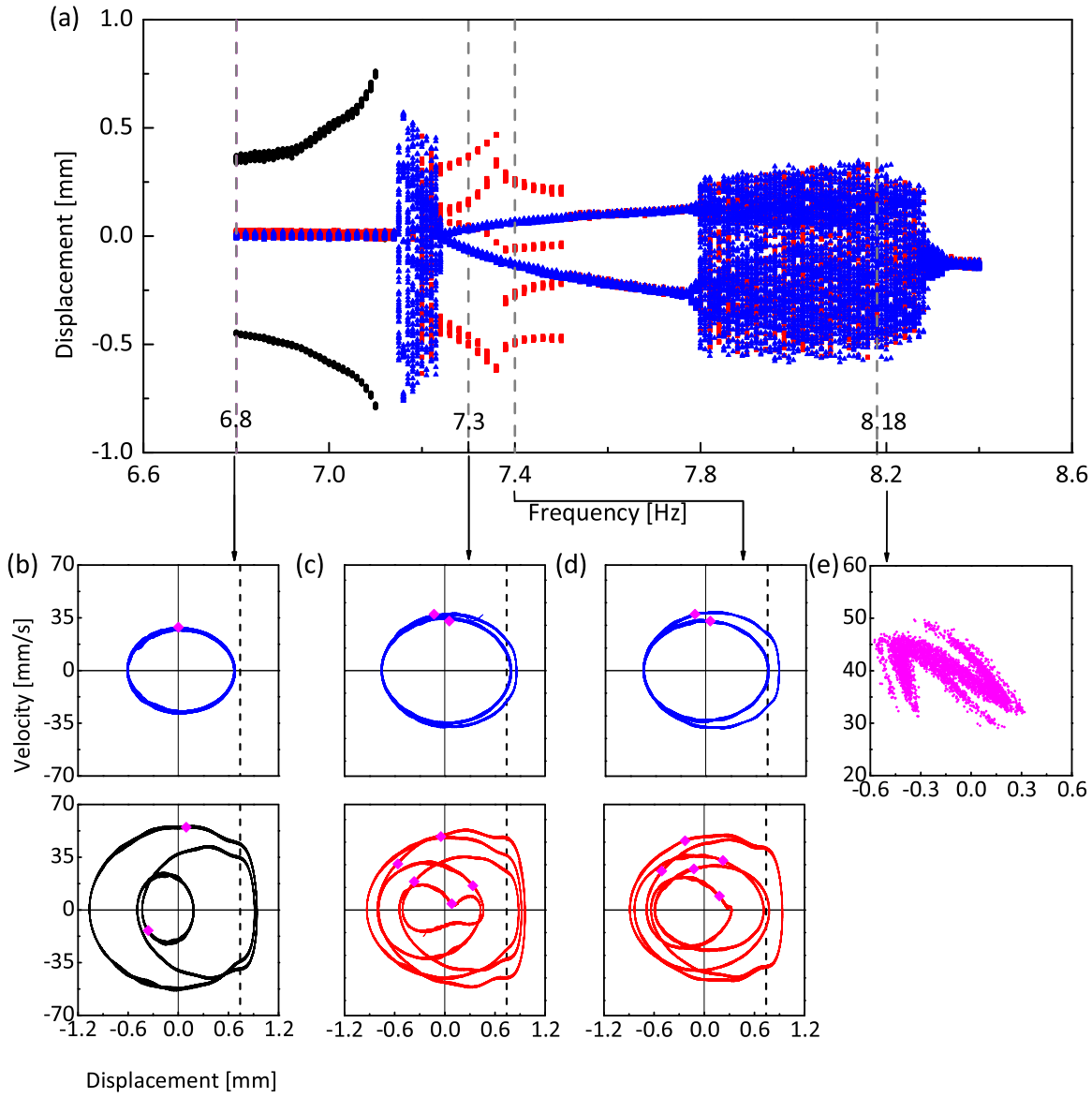

Fig. 2. Experimentally determined responses selected to test the orbit exchange control; (a) Bifurcation diagram constructed for the current amplitude of 1.45 A; and phase portraits of co-existing attractors recorded at (b) $f = 6.8$ Hz; (c) 7.3 Hz; (d) 7.4 Hz; (e) 8.18 Hz. Forward diagrams are traced in black circles (●) and blue triangles (▲), and backward diagrams are traced in red squares (■). Trajectories are presented by the respective colour of their attractors on the bifurcation diagram and Poincaré sections are depicted in magenta diamonds (◆). Dashed grey lines highlight these frequencies and dashed black lines represent the impact boundary.

Table 2
Overview of the selected cases to analyse TDF control and its limitations.

f [Hz]	Initial behaviour	First target	Second target	Original stability	Multiples	Success
6.8	Period-2	Period-1	Period-2	Stable	Yes	No
7.3	Period-5	Period-2	Period-5	Stable	No	Yes
7.4	Period-5	Period-2	Period-5	Stable	No	Yes
8.18	Chaos	Period-2	Period-1	Unstable	Yes	Yes

at $f = 6.8$ Hz, where period-1 and period-2 stable responses are targeted is chosen to illustrate the limitations of TDF control and the need for the new control method to perform the exchange in such cases.

Before the control method is applied, the chaotic attractor occurring at $f = 8.18$ Hz is considered in detail. Specifically, two embedded unstable periodic orbits (UPOs) to be targeted by the control are identified by constructing the Poincaré section of the chaotic attractor numerically and locating the unstable periodic orbits through the close return point method [53]. Fig. 3 shows the chaotic attractor and both UPOs identified by this method. The chaotic response is also verified by the calculation of its maximum Lyapunov exponent $\lambda_{max} = 4.14$ s^{-1}.

Finally, to complement the control analysis and have a more comprehensive overview of the system dynamics, we constructed the basins of attraction at the selected frequencies of $f = 6.8$ Hz and $f = 7.3$ Hz, as shown in Fig. 4. In both cases, the basins' boundaries are close to at least one point of the attractor, indicating that a relatively small deviation away from the attractor can make the system to migrate to another basin. This is beneficial to perform exchange between co-existing attractors as the controller is only required to generate a small disturbance.

3. Controlling exchange between co-existing attractors

In this section, we focus on the exchange of co-existing attractors starting with the TDF as well as the calculation of Floquet

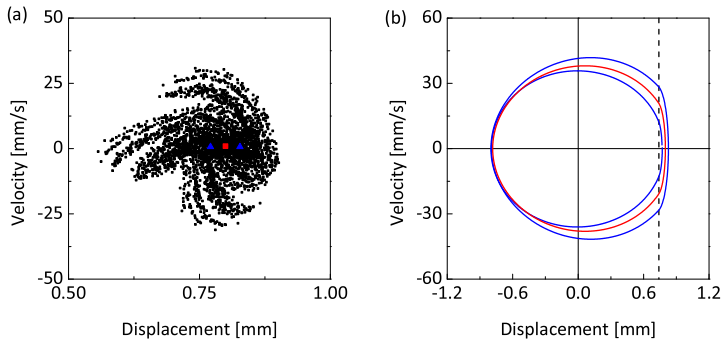

Fig. 3. (a) Poincaré map showing the chaotic attractor in black circles (●), identified period-1 UPO in red squares (■) and period-2 UPO in blue triangles (▲). (b) Phase portraits of the identified period-1 UPO in red and period-2 UPO in blue. The vertical dashed line represents the impact boundary.

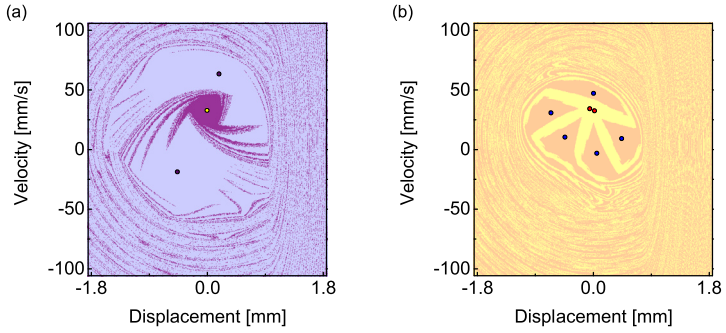

Fig. 4. Basins of attraction of the uncontrolled stable orbits. (a) Basin of the period-1 non-impacting orbit in purple (●) and period-2 impacting orbit in light purple (●) at $f = 6.8$ Hz, and their Poincaré maps in yellow (●) and dark purple (●) circles respectively; (b) Basin of the period-2 orbit in light yellow (●) and period-5 orbit (●) at $f = 7.3$ Hz, and their Poincaré maps in red (●) and blue (●) circles respectively.

exponents to evaluate orbits stability. Afterwards, the TDF control is applied to each case and its limitations are identified. Finally, we point out deficiencies of the TDF method in performing the exchange between orbits and justify a need for an enhanced control method.

3.1. Time-delayed feedback control

The time-delayed feedback control [24] was originally designed to stabilize unstable periodic orbits embedded into a chaotic attractor. Its main idea is to take advantage of the system dynamics to obtain a periodic orbit from a chaotic response by the feedback of delayed states instead of the present state of the system. A dynamical system with a delayed state control can be defined as follows [54]:

$$\begin{aligned} \dot{\mathbf{x}} &= \mathbf{f}(\mathbf{x}, t) + \mathbf{u}(\mathbf{y}(t), \mathbf{y}(t-\tau)), \\ \mathbf{y}(t) &= \mathbf{C}(\mathbf{x}), \end{aligned} \tag{4}$$

where $\mathbf{x}$ is the vector of state variables, $\mathbf{f}$ is the system time evolution function, $\mathbf{y}$ is the system observation provided by the function $\mathbf{C}(\mathbf{x})$, and τ is the delay. The control signal, $\mathbf{u}$, of the TDF method is defined as:

$$\mathbf{u} = \mathbf{K}(\mathbf{y}(t-\tau) - \mathbf{y}(t)), \tag{5}$$

where $\mathbf{K}$ is a proportional gain matrix. In the original formulation of the method [24], the delay τ is set to the period of the target unstable periodic orbit enabling the control signal to reduce to zero as the system approaches the targeted orbit as $\mathbf{y}(t-\tau) \rightarrow \mathbf{y}(t)$. The gain matrix $\mathbf{K}$ is normally set by analysing the target orbit stability where Lyapunov exponents or Floquet theory can be used. In the standard method, when the objective is to stabilize an unstable periodic orbit (UPO), the setting of the controller gains is crucial for its success and a proper analysis of the system response is needed.

Floquet theory is an efficient tool to describe the stability of periodic orbits as it only requires the analysis of one period of the evaluated response. If a deviation from a periodic orbit $\mathbf{x_{ob}}(t) = \mathbf{x_{ob}}(t-\tau)$ is given by $\delta\mathbf{x}(t) = \mathbf{x}(t) - \mathbf{x_{ob}}(t)$, Floquet theory can describe its evolution as:

$$\delta\mathbf{x}(t) = \mathrm{Re}\left(\sum_{n=1}^{N} (\delta\mathbf{x}(0) \cdot \mathbf{p_n}(0)) \exp(\mu_n t)\mathbf{p_n}(t)\right), \tag{6}$$

where μ_n is the nth Floquet exponent, $\cdot$ is the scalar product and $\mathbf{p_n}(t) = \mathbf{p_n}(t-\tau)$ is a periodic function with the same period as the system Jacobian $\nabla\mathbf{f}(x)$ evaluated around $\mathbf{x_{ob}}(t)$.

If all Floquet exponents have negative real parts, the exponential terms decrease with time while all other terms are limited, hence, $\delta\mathbf{x}$ tends to vanish as $t \rightarrow \infty$ indicating that $\mathbf{x_{ob}}$ is stable. On the other hand, if any of the Floquet exponents has a positive real part, the deviation $\delta\mathbf{x}(t)$ will increase with time and the solution may diverge from the orbit. Thus, the orbit stability can be evaluated by analysing the maximum real value of the Floquet exponents, defined as $\mathrm{Re}(\mu_{max}) \geq \mathrm{Re}(\mu_n)\ \forall\ n$. The orbit is stable if $\mathrm{Re}(\mu_{max}) \leq 0$.

When stabilizing UPOs, the calculation of Floquet exponents dictates the range of gains $\mathbf{K}$ where the controller can stabilize the orbit. For most mechanical systems only force can be used as an actuation. Thus, if we assume a single degree-of-freedom system and that $\mathbf{y} = \mathbf{C}(\mathbf{x}) = \mathbf{x}$, the resulting gain matrix will have the form:

$$\mathbf{K} = \begin{bmatrix} 0 & 0 \\ K_p & K_v \end{bmatrix}, \tag{7}$$

where K_p is the gain related to the feedback of position and K_v is the gain related to the feedback of velocities.

To illustrate this, we analyse the chaotic case at 8.18 Hz. Period-1 UPO real value of Floquet exponent (μ_{max}) is calculated

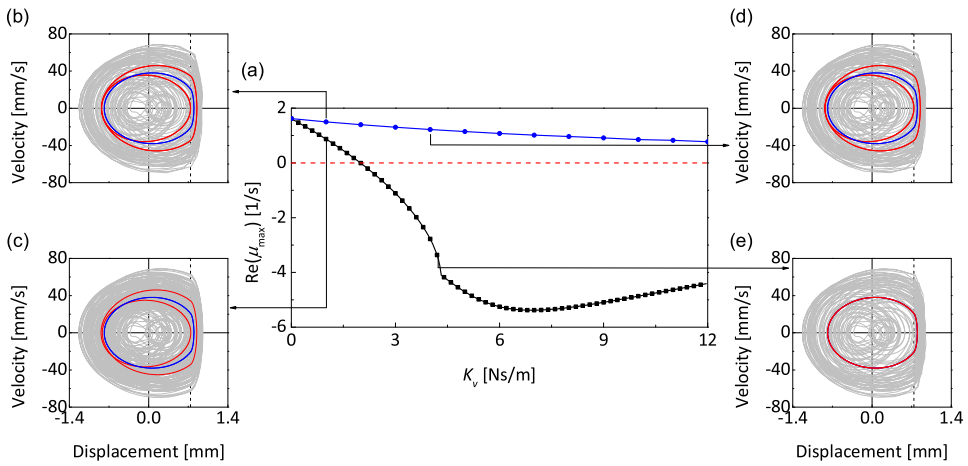

Fig. 5. Chaotic case stability analysis for the period-1 UPO. (a) Theoretical Floquet exponents varying the gain K_v and maintaining a constant $K_p = 0$ N/m, for $\tau = 1$ period of excitation in ■ and $\tau = 2$ periods of excitation in ●. The red dashed line highlights the boundary of stability. State space for the initial response (grey), target response (blue) and stabilized response (red) for control parameters (b) $K_v = 1.0$ N s/m and $\tau = 2$ periods; (c) $K_v = 1.0$ N s/m and $\tau = 1$ period; (d) $K_v = 3.2$ N s/m and $\tau = 2$ periods; (e) $K_v = 3.2$ N s/m and $\tau = 1$ period. The dashed vertical black line indicates the impact boundary.

by an optimization method described in Appendix for various values of the gain K_v and fixed $K_p = 0$. Fig. 5(a) shows the computed real value of μ_{max} for a delay of one period, shown by a black curve, and the values for a delay of two periods, shown by a blue curve. For the case of delay of one period, two important values of the gain K_v should be highlighted. The first value of 2.0 N s/m indicates the lowest value of K_v where the TDF can stabilize the orbit and the value of 6.6 N s/m is where the maximum Floquet exponent μ_{max} reaches its minimum, which indicates that the orbit has its maximum stability. Fig. 5(c) shows the state space of the system response when the gain is too low to stabilize the target period-1 UPO, in blue, and the controlled system ends up in a different response, in red, whist Fig. 5(e) shows a successful control as the gain K_v is in the stability region and the target and controlled orbit overlap with each other. Also, if the delay of the controller is set to be two periods of excitation, the μ_{max} of the period-1 UPO becomes positive indicating that the orbit is unstable. This can be clearly be seen in Fig. 5(b) and (d) which show the failed stabilization of the correct period-1 target response and the stabilization of a period-2 UPO even though the system was initiated in the period-1 UPO.

If the objective of the control is to perform the exchange between already stable orbits, the analysis of the Floquet exponents becomes less crucial and gains can be set on a trial and error basis by choosing a low initial value of gains and slowly raising them until the controller has enough energy to guide the system to the desired response. This procedure allows the control method to successfully perform the exchange between two periodic orbits with only the required information being the knowledge of the co-existence of the solutions and the target orbit period.

Finally, a special problem with TDF should be mentioned when dealing with the exchange of co-existing solutions. Imagine that the system is settled on a stable periodic orbit of period τ_s ($\mathbf{x}(t-\tau_s) = \mathbf{x}(t)$), and the TDF control targets another co-existing periodic orbit with period $j\tau_s$ where $j \in \mathbb{N}$ ($\mathbf{x}(t-j\tau_s) = \mathbf{x}(t)$). In this case, the control signal would be from Eq. (5):

$$\mathbf{u} = \mathbf{K}(\mathbf{y}(t-j\tau_s) - \mathbf{y}(t)). \tag{8}$$

However, as the system is initially exhibiting a periodic orbit that obeys $\mathbf{x}(t-j\tau_s) = \mathbf{x}(t-(j-1)\tau_s)$, and consequently $\mathbf{y}(t-j\tau_s) = \mathbf{y}(t-(j-1)\tau_s)$, the control signal will be zero as:

$$\begin{aligned}\mathbf{K}(\mathbf{y}(t-j\tau_s) - \mathbf{y}(t)) &= \mathbf{K}(\mathbf{y}(t-(j-1)\tau_s) - \mathbf{y}(t)) \\ &= \cdots = \mathbf{K}(\mathbf{y}(t-\tau_s) - \mathbf{y}(t)) = \mathbf{0}.\end{aligned} \tag{9}$$

This is a drawback for the exchange using TDF in such cases as the control signal will be zero or very small if there is some deviation from the initial orbit or noise. Thus, TDF cannot easily make the current orbit unstable.

If the initial behaviour of the system is an UPO with period τ_s which is then stabilized by the TDF control, the controller might be able to perform the exchange to another period $j\tau_s$ orbit. The exchange can happen if the initial UPO loses its stability under the new control signal as the controller parameters change. In these conditions, the system would naturally move away from the initial periodic orbit and the TDF control signal would be able to lead the system to the desired response. However, it is important to emphasize that these specific conditions are difficult to obtain and generally require a much greater knowledge of the system dynamics to set the controller gains. Another possibility is to simply turn the control off and wait for the system to naturally diverge from the initial orbit and turn the control on again targeting the desired solution. The latter option can be applied to all unstable cases, but it still requires the chaotic response to be resumed and a good knowledge of the system dynamics.

3.2. TDF results and limitations

The ability of the TDF method to perform an exchange between solutions is tested both numerically and experimentally. This is done by studying various cases chosen to assess the advantages and disadvantages of the method. In all considered cases, the control signal is given by:

$$\mathbf{u} = \begin{bmatrix} 0 \\ aI_{act} \end{bmatrix} = \begin{bmatrix} 0 & 0 \\ K_p & K_v \end{bmatrix} \cdot \begin{bmatrix} x(t-\tau_s) - x(t) \\ \dot{x}(t-\tau_s) - \dot{x}(t) \end{bmatrix}, \tag{10}$$

as the actuation current is the only accessible parameter.

The cases are sequenced and presented with an increasing difficulty for a successful exchange of attractors, as summarized by Table 2. The cases at $f = 7.3$ and 7.4 Hz are initially presented, where the co-existing attractors do not have periods that are multiples of themselves. Afterwards, the more difficult cases at $f = 8.18$ and 6.8 Hz are presented where the attractors have periods which are multiples of themselves.

In the cases where the TDF performs an exchange between stable attractors, the Floquet exponents of the orbits are not used to set controller gains as the stability of these attractors is already assured. Hence, only the knowledge of the target orbits period is considered in these cases and the controller gains are set on the

trial and error basis by the following method. First, the system starts with an undesired response and the controller gains are set to zero. Then, the control is turned on and the controller gains are slightly increased to evaluate whether if the controller has enough energy to bring the system to the desired response. If the desired orbit is reached, the gains are set to their current value and the procedure stops. If there is no exchange, the gains are slightly raised again. This procedure is repeated until the successful exchange is achieved or if the gains exceed the experimental safety limits, namely $I_0+I_{act} < 4$ A and $|X| < 6$ mm, which means that the controller cannot experimentally perform the exchange. In all cases, experimental results are obtained using the rig configuration as reported in [22]. Experimental Poincaré sections and control experiments are constructed with the acquisition frequency set as a multiple of the excitation frequency to eliminate any drift or error related to the mismatch between them. Also in experiments, time windows are multiple of excitation periods and are set manually. Numerical results are calculated by using a fourth-order Runge Kutta method where the excitation amplitude and initial conditions are taken directly from the experiments.

First, the case of $f = 7.3$ Hz is considered with the aim to explore if the control can switch back and forth between the coexisting period-2 and period-5 orbits. The test starts with the system exhibiting the period-5 orbit, and then the controller is turned on targeting the period-2 orbit with controller gains and delay $K_p = 8.0$ N/m, $K_v = 3.2$ N s/m and $\tau = 2/f = 0.2740$ s. After a successful switch is reached, the controller changes its target to the previous period-5 orbit with controller parameters $K_p = 159.86$ N/m, $K_v = 3.2$ N s/m and $\tau = 5/f = 0.6849$ s. The results are shown in Fig. 6 where the exchange between both orbits is modelled numerically and experimentally confirmed. Numerical time histories of response and control signal, shown in Fig. 6(a) and (b), demonstrate a fast switch to the period-2 orbit, shown in Fig. 6(c), which was achieved with a small control signal and a relatively short transition time of about 50 periods. The transition to the period-5 orbit, shown in Fig. 6(d), is initially dominated by an unstructured response that lasts for about 100 excitation periods and ends when the system begins to exponentially converge to the period-5 orbit. This long transition suggests a difficulty of the TDF to move the orbit away from the period-2 orbit basin of attraction and reach the basin of the period-5 attractor, even though only a small disturbance of the state space is required to change to the other basin, as shown in Fig. 4(b). The corresponding experimental time histories presented in Fig. 6(e) and (f), exhibit the same behaviour as numerical results when the period-2 orbit, shown in Fig. 6(g), is targeted. The only exception is that the experiments require a slightly larger control signal than the numerical simulation. During the transition to the period-5 orbit, shown in Fig. 6(h), the experimental results demonstrate a smaller intermediary phase, but a longer convergence phase and a larger control signal than the numerical results, leading to a longer transition time. These slight differences from numerical results can be related to the noise in the experimental controller and time intervals where the control signal is constant due to the data acquisition system saving data. Overall, using the TDF method and the strategy presented, one can successfully perform the exchange between the attractors without major problems both numerically and experimentally.

Now the case of excitation frequency $f = 7.4$ Hz is considered, where the control strategy outlined above encountered problems. Specially, we were not able to find a gain that would move the system away from the period-2 orbit and stabilize the period-5 orbit, hence, a modified strategy was developed. Initially, the system exhibits the period-5 response and the control targets the period-2 orbit with gains of $K_p = 1.8$ N/m and $K_v = 3.2$ N s/m, and delay of $\tau = 2/f = 0.2703$ s. Once the period-2 orbit is reached, the controller gains are changed to push the system away from the period-2 orbit, starting the transition phase that lasts for 50 periods, for controller parameters of $K_p = 159.86$ N/m, $K_v = 1.8$ N s/m and $\tau = 5/f = 0.6757$ s. Afterwards, the gains are changed again to $K_p = 1.8$ N/m and $K_v = 3.2$ N s/m initiating the targeting phase, where the controller helps the system reach the period-5 orbit. The test is shown in Fig. 7, where numerical time histories of position and control signal, shown in Fig. 7(a) and (b), demonstrate that the controller can easily perform the exchange from the period-5 to the period-2 orbit, shown in Fig. 7(c), with a very short transition time of about 20 periods and a small control signal. Afterwards, the controller changes its target and enters its transition phase when it moves the system away from the period-2 orbit. This is marked by the higher control signal around 80 s. After the transition phase is finished, the controller changes to the targeting phase where the control signal drops significantly and the system converges to the period-5 orbit, shown in Fig. 7(d), in about 100 periods. The corresponding experimental results, shown in Fig. 7(e) and (f), demonstrate that the controller initially takes a longer time to reach the period-2 orbit, shown in Fig. 7(g), when compared with numerical simulation, resulting in an exchange time of about 150 periods. Afterwards, the controller changes its target and enters its transition phase. Subsequently, the controller reaches its targeting phase and the system converges to the period-5 orbit with a slightly longer convergence time than in numerical simulations of about 75 periods and a slightly larger control signal.

This second scenario demonstrates that the TDF method can experience some difficulties to switch between orbits and even though raising gains can be used as a strategy, it can lead to several difficulties, such as destabilizing the target orbit. It also seems that the controller has more difficulties to perform the exchange from a low period orbit to a high period one than vice-versa. This limitation motivates us to look for other control strategies.

More challenging cases are now considered where the coexisting attractors have periods that are multiple among themselves, such as period-1 and period-2 orbits. Initially, the case of excitation frequency $f = 8.18$ Hz is analysed where the system presents a chaotic response. This scenario should be more advantageous for the TDF method than the scenario of $f = 6.8$ Hz as the target orbits are unstable. Also, in the chaotic case, it is assumed that there is a full knowledge of both target orbits. In other words, a perfect case is analysed where the period-1 UPO Floquet exponents can be used to set the controller gains. Two objectives are set here, to investigate if the TDF can promote the stabilization and exchange between the identified period-1 and period-2 UPOs in the given time windows and to confirm if the model and numerical predictions of Floquet exponents can be used to set experimental controller parameters.

As previously shown in Fig. 5 the change of time-delay alone is theoretically sufficient to perform the switch between UPOs due to the instability of the period-1 orbit when the delay is set to two periods of excitation. Thus, the same gain K_v is used for both orbits and set in such a way that the orbit would have μ_{max} around the minimum value, where the orbit is most stable, and also be small, resulting in $K_v = 3.2$ N s/m and $K_p = 0$ N/m. The exchange is then performed by adjusting the time delay τ to the period of the target orbit. The system initially presents a chaotic response as the control is turned off. Afterwards, the control is turned on to stabilize the period-2 UPO, with $\tau = 2/f = 0.2445$ s. If stabilization is achieved, the controller waits a few seconds and then moves its target to the period-1 UPO with $\tau = 1/f = 0.12225$ s. If it is successful in stabilizing the period-1 UPO, the controller readjusts its delay targeting again the period-2 UPO to

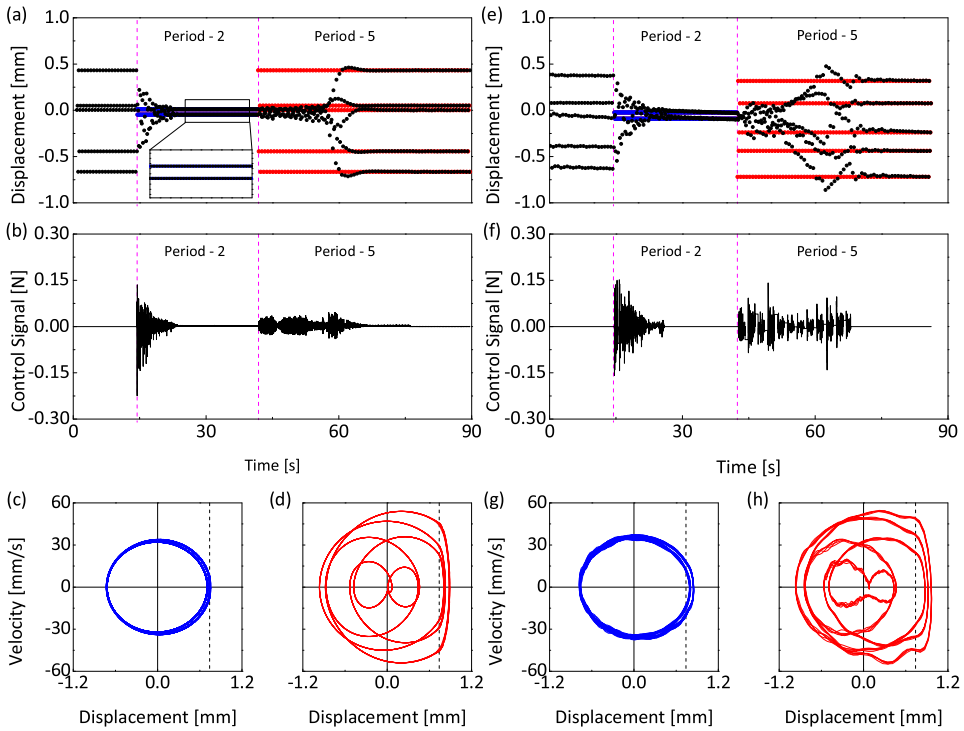

Fig. 6. Example of successful application of the TDF control for the case of $f = 7.3$ Hz. The system response is presented in black (●), period-2 target response in blue (●) and period-5 target response in red (●). (a–d) Numerical results and (e–h) experimental results. Dashed vertical magenta lines represent the exact moments when the controllers change their target orbit, while dashed black lines represent the impact boundary. (a),(e) Poincaré stroboscopic time history of displacement. The two paths indicating a period-2 orbit can be distinguished on the highlight of panel (a). (b),(f) Control signal time history. (c),(g) Numerical and experimental period-2 orbits respectively. (d),(h) Numerical and experimental period-5 orbits respectively.

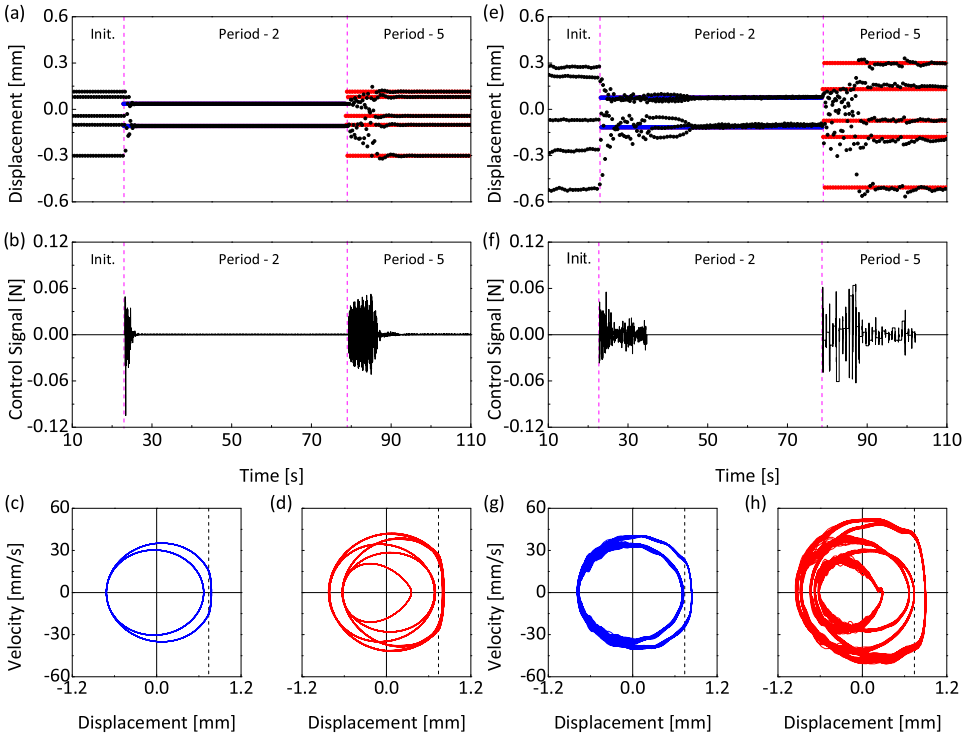

Fig. 7. Example of successful application of the TDF control for the case of $f = 7.4$ Hz. The system response is presented in black (●), period-2 target response in blue (●) and period-5 target response in red (●). (a–d) Numerical results and (e–h) experimental results. Dashed vertical magenta lines represent the exact moments when the controllers change their target orbit, while dashed black lines represent the impact boundary. (a),(e) Poincaré stroboscopic time history of displacement. (b),(f) Control signal time history. (c),(g) Numerical and experimental period-2 orbits respectively. (d),(h) Numerical and experimental period-5 orbits respectively.

test if it can perform the exchange in reverse. Finally, the control is turned off so the system can regain its chaotic state.

Fig. 8 shows the numerical and experimental results for the described strategy. Numerical results, shown in Fig. 8(a) and (b),

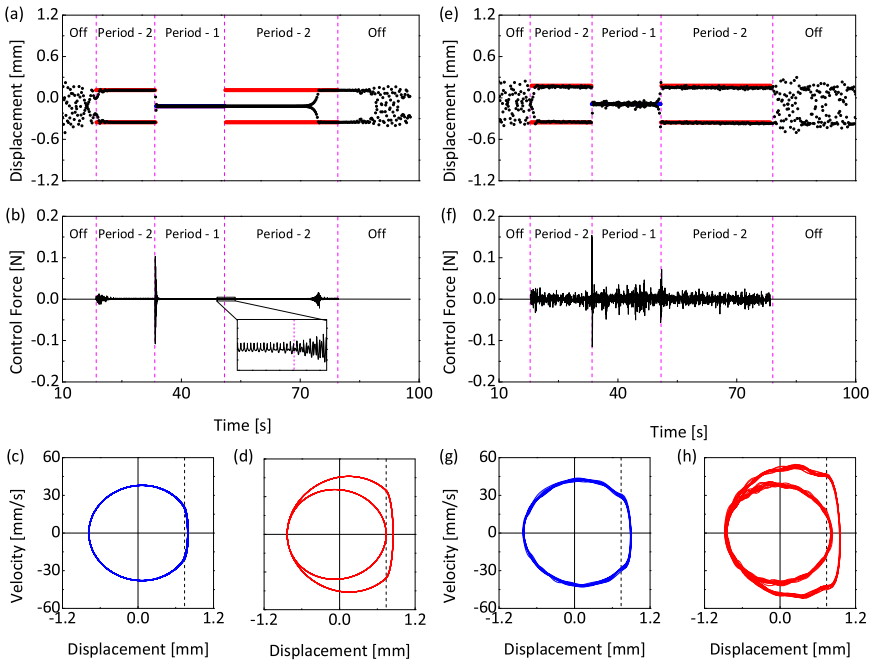

Fig. 8. Example of successful application of the TDF control for the chaotic case of 8.18 Hz. The numerical case presents some difficulties to perform the exchange from period-1 to period-2 orbits. The system response is presented in black (●), period-1 target UPO in blue (●) and period-2 UPO in red (●). (a–d) Numerical results and (e–h) experimental results. Dashed vertical magenta lines represent the exact moments when the controllers change their target orbit, while dashed black lines represent the impact boundary. (a),(e) Poincaré stroboscopic time history of displacement. (b),(f) Control signal time history. (c),(g) Numerical and experimental period-1 UPOs respectively. (d),(h) Numerical and experimental period-2 UPOs respectively.

initially display a chaotic response as the control is turned off. After the control is switched on targeting the period-2 UPO, the system rapidly stabilizes on the target orbit with a very small control signal. After stabilization is achieved, the controller changes its time delay targeting the period-1 UPO, shown in Fig. 3(c), and rapidly brings the system to the desired response. Next, the controller changes again its time delay targeting the period-2 UPO, shown in Fig. 3(d), and it takes more than 200 periods to ramp up its signal and perform the exchange. Finally, the control is turned off and the system returns to its chaotic state. The long period of time needed to perform the exchange is explained by Eq. (9) as the control signal continues to be very small. After some time the system moves away from the period-1 UPO due to the change in stability caused by the controller delay modification, this leads to a small deviation of the orbit and allows the control signal to slowly ramp up, which can be seen in the detail panel of Fig. 8(b), and perform the exchange to the period-2 UPO. The experimental results, shown in Fig. 8(e) and (f), present the same behaviour as the numerical up to the transition to the period-2 UPO. At this point, the experimental control diverges from the numerical as it can rapidly perform the transition to the period-2 UPO. This is due to the presence of noise that creates greater deviations of the period-1 orbit enabling the control signal to ramp up faster than in numerical simulations and quickly perform the exchange. This can be confirmed numerically by adding a Gaussian noise to the control force, with variance calculated from the experimental data of 0.0102 N. In this case, the numerical results also indicated a faster transition from the period-1 UPO to the period-2 UPO. It is also important to note that noise in the system is greater in the chaotic response than in all the periodic responses. Hence, it should be emphasized that even with a higher than 20% noise over maximum signal ratio, the controller can stabilize both UPOs which demonstrates robustness of the controller when controller parameters are set to maximize the UPO stability. Finally, the experimental stabilization of both UPOs with a high noise to signal ratio shows the possibility of setting experimental controller gains by minimizing the real value of the predicted maximum Floquet exponent of a UPO.

The Floquet exponents can be also estimated using experimentally recorded Poincaré time history as proposed by Costa et al. [38]. This method gives $\mathrm{Re}(\mu_{max}) = -0.94\ \ \mathrm{s}^{-1}$, for the period-1 UPO and $\mathrm{Re}(\mu_{max}) = -1.16\ \ \mathrm{s}^{-1}$ for the period-2 UPO. The period-1 $\mathrm{Re}(\mu_{max})$ calculated for experiments is much higher than its numerical counterpart of $-5.16\ \ \mathrm{s}^{-1}$ but it is still negative. Thus, it is likely that noise and other experimental imperfections raised the value of the controlled orbit Floquet exponent but the change was not sufficient to make the exponent positive and so the UPO stabilization was successful.

The last case of excitation frequency of $f = 6.8$ Hz is now explored. Here the control strategy is to target the period-1 non-impacting orbit with gains $K_p = 159.86$ N/m and $K_v = 2.42$ N s/m, and controller delay $\tau = 1/f = 0.147$ s. Once period-1 orbit is reached, the co-existing period-2 orbit is targeted initially with the same gains $K_p = 159.86$ N/m and $K_v = 2.42$ N s/m, and controller delay $\tau = 2/f = 0.294$ s. Numerical results, shown in Fig. 9(a) and (b), demonstrate that the controller can perform the switch to the period-1 non-impacting orbit, shown in Fig. 9(c), easily with a very small transition time and control signal, however, it cannot bring the system from the period-1 to the period-2 response, shown in Fig. 9(d). For the experimental case, shown in Fig. 9(e) and (f), the controller also can stabilize the period-1 orbit, shown in Fig. 9(g), with a greater transition time than in the numerical simulations due to noise. However, the controller is not able to perform the exchange from the non-impacting to the impacting orbit, even though the difficulty to exchange between orbits according to the basins of attraction, shown in Fig. 4, is the same as the successful case at $f = 7.3$ Hz. In fact, there was no value of controller gains allowing the controller to perform the exchange without destabilizing the whole system and producing displacements greater than the safety limits for the experiment. This difficulty is explained by the fact that even if a small deviation from the initial orbit is achieved, it will still

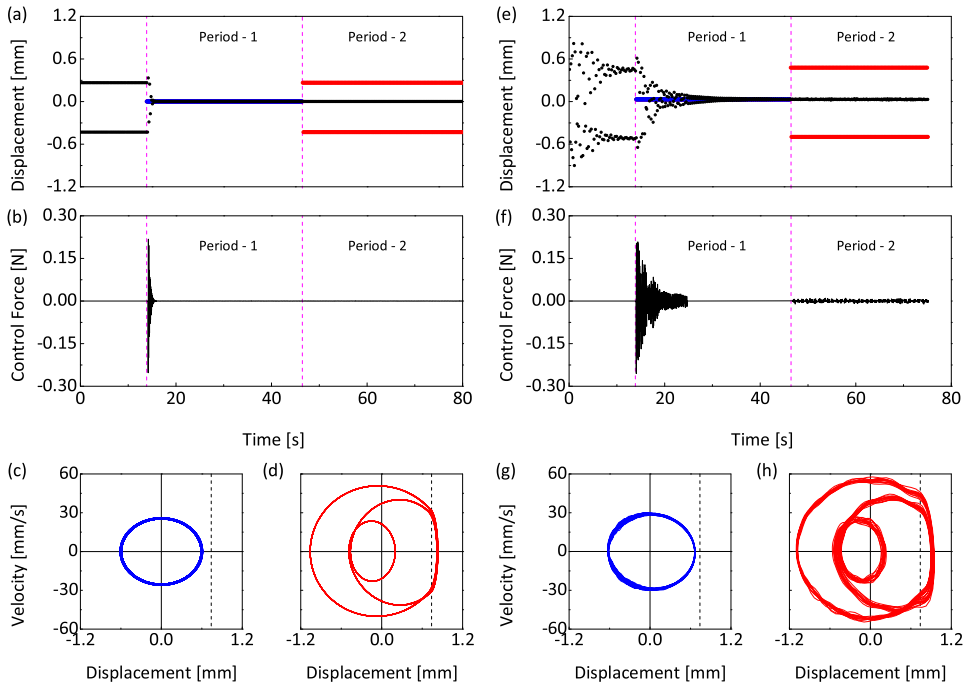

Fig. 9. Example of unsuccessful application of the TDF control for the case of 6.8 Hz. The TDF method alone could not perform the exchange from the period-1 stable orbit to the period-2 orbit. The system response is presented in black (●), target period-1 response in blue (●) and period-2 response in red (●). (a–d) Numerical results and (e–h) experimental results. Dashed vertical magenta lines represent the exact moments when the controllers change their target orbit, while dashed black lines represent the impact boundary. (a),(e) Poincaré stroboscopic time history of displacement. (b),(f) Control signal time history. (c),(g) Numerical and experimental period-1 orbits respectively. (d),(h) Numerical and experimental period-2 orbits respectively.

vanish due to the stability of the orbit, which does not allow the control signal to grow.

This last case of 6.8 Hz demonstrates that manipulating the gain of the TDF method to move away from a periodic attractor and destabilize a periodic orbit in some cases is not a viable option. In addition, high gain values might not be possible to achieve due to the actuators limitations. Hence a new approach should be implemented to perform the exchange from a period-n stable orbit to a period-jn stable orbit.

4. Fractional time-delayed feedback control

In this section, a new method based on the TDF control is proposed to switch from a stable period-n orbit with period τ_s to another co-existing period-jn orbit. The idea is to initially change the controller time-delay to a fraction of τ_s aiming to destabilize the current periodic response and to move the system away from the current attractor. Once the system response is away from the initial attractor, the controller time delay is set to the period of the targeted periodic orbit. This method is more advantageous than just increasing the controller gain $\mathbf{K}$ as this can lead to instability, great increases in vibration amplitude and high control signal.

As it was suggested previously [36,55,56], the detuning of TDF's time delay from the current response period leads to destabilization of the orbit and the creation, by the controller, of a periodic or chaotic attractor that is constrained in a closed region of the state space. Hence, if it is affordable for the system to exhibit a bounded unknown response for a short period of time, this can be a viable option to take the system state away from an unwanted attractor. It is also important to highlight that there is no additional information needed to implement this new method, than the one already needed for the TDF approach.

Hence, the controller is defined by two stages where the first stage uses a fractional time-delay to move away from an initial orbit and the second uses the actual period of the target orbit to bring the system to the desired response, leading to the control rule given by:

$$\mathbf{u}(t) = \begin{cases} \mathbf{K}\cdot(\mathbf{y}(t-\frac{\tau_s}{q}) - \mathbf{y}(t)) & \text{, if } t < t_{trans} \\ \mathbf{K}\cdot(\mathbf{y}(t-j\tau_s) - \mathbf{y}(t)) & \text{, otherwise,} \end{cases} \tag{11}$$

where t_{trans} is a time window large enough to bring the system away from the periodic orbit and $q > n, q \in \mathbb{N}$ is a detuning coefficient. The condition of $q > n$ is in place so lower period orbits are not targeted. For example, if the system response is a period-2 orbit, $n = 2$, and the target is a period-4 orbit, a detuning coefficient $q = 2$, $q = n$, can promote the exchange to a period-1 co-existing orbit, if it exists, which in turn, will present the same problem to the control second stage, thus preventing the exchange to the targeted period-4 orbit. The time t_{trans} can be set as the time needed for the system to present a steady state response or the time needed for the system to go to another basin of attraction if basin's boundaries are known. Other criteria can be a threshold distance in the state space between the original orbit and the targeted response of the system. Finally to set the gains of this controller, one can apply the same strategy as was previously used for the TDF method in the cases with stable orbits.

An example of FTDF control implementation is visualized in Fig. 10. In the first stage, the half period delay creates a periodic control signal, shown in Fig. 10(a), which stabilizes the system on an attractor presented in Fig. 10(b) in black. When the second stage is reached, this control generated attractor is destroyed as the control signal changes and the system is pushed to the period-2 orbit given in red as the control signal decreases to zero. In other words, the first stage generates an attractor that is not part of the system original behaviour, which is used as a bridge to perform the exchange from the period-1 (blue) to the period-2 (red) orbit. It is important to highlight that the control generated attractor, may not be a period-1 orbit as presented in the example, but will be bounded to a region of the state space.

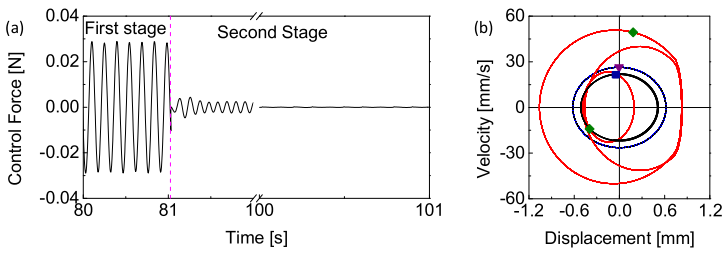

Fig. 10. An example highlighting the fractional period phase of the FTDF method. (a) Control signal time history showing the first stage when the system reaches the control generated attractor, the beginning of the second stage when the system leaves the control generated attractor and the end of the second stage when the system is already settled on the target orbit. (b) Phase portraits of the original period-1 (blue) and target period-2 (red) orbits and control generated attractor (black) created in the transition stage, Poincaré sections are in purple triangles, green diamonds and navy squares respectively.

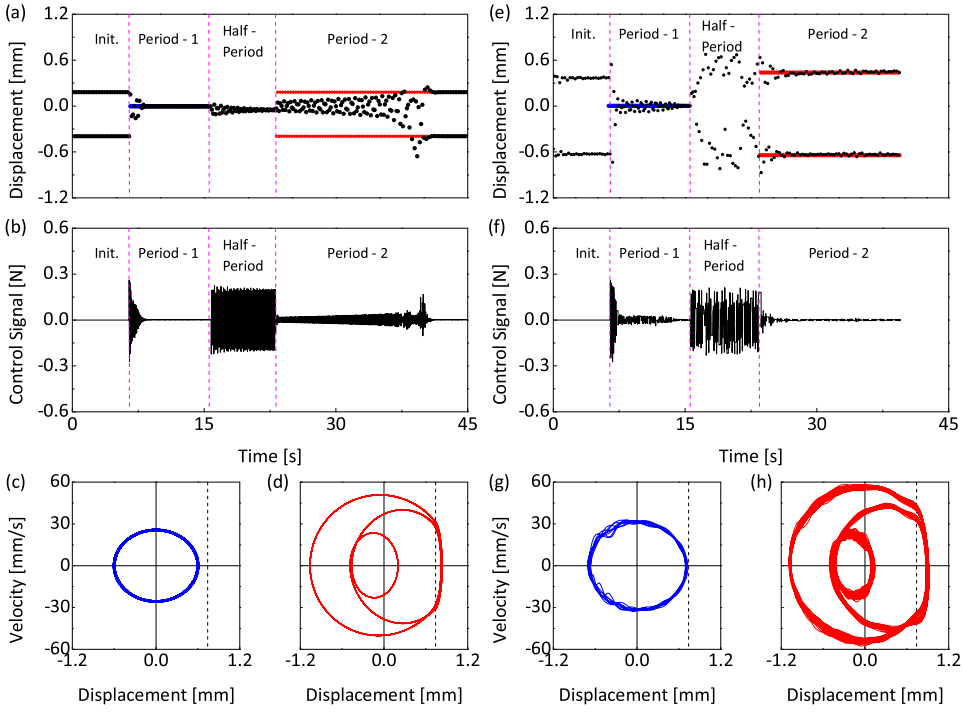

Fig. 11. Example of successful application of the FTDF control for the case of $f = 6.8$ Hz, where TDF alone cannot perform the exchange. The system response is presented in black, target period-1 response in blue and period-2 response in red. (a–d) Numerical results and (e–h) experimental results. Dashed vertical magenta lines represent the exact moments when the controllers change their target orbit, while dashed black lines represent the impact boundary. (a),(e) Poincaré stroboscopic time histories of displacement. (b),(f) Control signal time histories. (c),(g) Numerical and experimental period-1 orbits respectively. (d),(h) Numerical and experimental period-2 orbits respectively.

To demonstrate the implementation of this new method both experimentally and numerically, the case of $f = 6.8$ Hz is revisited. The control strategy is the same as described before when applying the standard TDF control for the same scenario. The controller is set with the same gains of $K_p = 159.86$ N/m and $K_v = 2.42$ N s/m so a comparison can be made between the TDF and the new method. The fractional time-delayed feedback control is only used in the transition to the period-2 orbit with $q_{trans} = 2$ and $t_{trans} = 50$ periods.

Fig. 11 shows the experimental and numerical results demonstrating implementation of the new FTDF method. In numerical simulations, shown in Fig. 11(a) and (b), the controller performs the exchange to the period-1 (Fig. 11(c)) and to the period-2 orbit (Fig. 11(d)) with a small control signal. In the half period phase, the controller has a bounded control signal that moves the system away from the period-1 orbit and stabilizes another control generated period-1 orbit. This shift is enough for the targeting phase to rump up the control signal and bring the system to the desired period-2 orbit within 120 excitation periods. Experimental results, shown in Fig. 11(e) and (f), demonstrate that the controller is also able to perform the switch between these two orbits. As can be seen from Fig. 11(c), in the fractional control first stage, the controller does not stabilize a control generated period-1 orbit as was expected from numerical simulation but instead it actually brings the system response closer to the period-2 orbit. Hence, in the targeting phase, the experimental control stabilizes the target response much more quickly than it is done in the simulations. These differences are likely to be the effects of noise as postulated for other cases. It is important to mention that normally the noise would extend the transition time which is evident in the transition from the period-2 to the period-1 orbit.

This brief analysis indicates that the FTDF control can successfully switch between periodic orbits in the case where the original TDF control has failed. It also demonstrates that this method has more advantages than simply raising controller gains due to reaching the required orbit with a limited control signal. However, it is important to highlight that if restrictions are applied to the control signal even the FTDF method may not be able to perform the exchange due to a strong stability of the original orbit.

5. Conclusions

Ability to switch between co-existing attractors can bring adaptability and new features to an engineering system, but only a few control methods can exchange back and forth between co-existing orbits. In this work, a versatile and highly controllable impact oscillator [21,22], developed in by the Centre for Applied Dynamics Research at the University of Aberdeen, is chosen to implement the TDF control methods and investigate its capabilities both numerically and experimentally. Four different cases were selected to examine the performance of the TDF control methods. In the first two cases, the TDF method performed the exchange between period-5 and period-2 attractors well, but showed some difficulties to switch from a low to a high period orbit. The third case displayed a difficulty when stabilizing and exchanging between unstable periodic orbits embedded in the chaotic attractor with periods that are multiples among themselves. The last case demonstrated the limitations of the classical TDF method as the controller was not able to safely switch from a period-1 to a co-existing period-2 orbits.

To address the last problem encountered, a new Fractional Time-Delayed Feedback Control (FTDF) was proposed and tested. The FTDF method is a two-stage control, where a control generated orbit is created and used as a bridge to switch between its initial and control targeted orbits. In the first stage, it uses a fraction of the initial orbit period to destabilize the current attractor and to establish a control generated orbit. In the second stage, the classical TDF approach is applied to bring the system to the desired attractor. From our limited testing experience it appears that the proposed control method presents a significant advantage of creating bounded responses during the exchange of attractor process.

The new FTDF method should be extensively tested to fully assess its effectiveness and robustness. However, the initial results look attractive as the method can be applied to various adaptive non-linear systems and structures where their behaviour or configuration is required to change.

CRediT authorship contribution statement

Dimitri Costa: Conceptualization, Methodology, Validation, Investigation, Formal analysis, Writing – original draft. **Vahid Vaziri:** Conceptualization, Formal analysis. **Ekaterina Pavlovskaia:** Visualization, Writing – review & editing. **Marcelo A. Savi:** Resources, Writing – review & editing, Supervision, Funding acquisition. **Marian Wiercigroch:** Resources, Writing – review & editing, Supervision.

Declaration of competing interest

The authors declare the following financial interests/personal relationships which may be considered as potential competing interests: Dimitri Danulussi Alves Costa reports financial support was provided by Coordination of Higher Education Personnel Improvement. Marcelo Savi reports financial support was provided by Carlos Chagas Filho Foundation for Research Support of Rio de Janeiro State. Dimitri Danulussi Alves Costa reports financial support was provided by National Council for Scientific and Technological Development.

Acknowledgements

The authors also acknowledge the financial support from Coordenação de Aperfeiçoamento do Pessoal de Nivel Superior (CAPES), under the Grant Number 88881.189487/2018-01 and FAPERJ.

Appendix. Calculation of Floquet exponents with time-delayed states

In this appendix, two methods of calculation of an unstable periodic orbits Floquet Exponents are described, following the approach presented in [38,54]. Floquet theory focuses on the behaviour of time-varying systems described by the differential equation:

$$\dot{\mathbf{x}} = \mathbf{M} \cdot \mathbf{x} \tag{A.1}$$

where $\mathbf{M}$ is a periodic matrix with period τ_s. In other words, $\mathbf{M}(t) = \mathbf{M}(t + \tau_s)$. As stated by Floquet theory, the result of Eq. (A.1) is given by:

$$\mathbf{x}(t) = \mathrm{Re}\left(\sum_{n=1}^{N} (\mathbf{x}(0) \cdot \mathbf{p_n}(0)) \exp(\mu_n t)\mathbf{p_n}(t)\right) \tag{A.2}$$

where $\mathbf{p_n}$ is a periodic function with the same period as $\mathbf{M}$ and μ_n is the Floquet exponent associated with $\mathbf{p_n}$ as explained in Section 3.1.

The first method of calculation considers a system controlled by the TDF method as in Eq. (4) that has a periodic behaviour $\mathbf{x_{ob}}$ of period τ_s. In this case, the time evolution of a deviation $\delta\mathbf{x}$ can be given through a linearization of Eq. (4) resulting in:

$$\delta\dot{\mathbf{x}} = (\nabla\mathbf{f}(\mathbf{x_{ob}}) + \mathbf{K}\nabla\mathbf{C}\,(\nabla\mathbf{x}(t - n\tau_s) - \mathbb{I})) \cdot \delta\mathbf{x} \tag{A.3}$$

where $\mathbb{I}$ is the identity matrix and ∇ is the gradient operator.

Note that Eq. (A.3) when evaluated around $\mathbf{x_{ob}}$ has the same form of Eq. (A.1) and the matrix $\mathbf{M}$ has a periodic behaviour with the same period τ_s as the orbit. Hence, Floquet theory can be applied which dictates that delayed deviations must have the form:

$$\delta\mathbf{x}(t - \tau_s) = \exp(-\mathbf{H}_\mu\tau_s) \cdot \delta\mathbf{x}(t) \tag{A.4}$$

where $\mathbf{H}_\mu$ is a matrix which its eigenvalues are the Floquet exponents. Using this result Eq. (A.3) becomes:

$$\delta\dot{\mathbf{x}} = (\nabla f(\mathbf{x_{ob}}) + \mathbf{K}\nabla\mathbf{C}(\mathbf{x_{ob}})(\exp(-\mathbf{H}_\mu\tau_s) - \mathbb{I})) \cdot \delta\mathbf{x} \tag{A.5}$$

Now that the evolution of $\delta\mathbf{x}$ is known, one way to calculate the Floquet exponents is to evaluate the fundamental matrix of the system Ψ that is defined as:

$$\delta\mathbf{x}(t) = \Psi(t) \cdot \delta\mathbf{x}(0) \tag{A.6}$$

where $\Psi(0) = \mathbb{I}$. In sequence, by substituting Eq. (A.6) into Eq. (A.5) the evolution of the fundamental matrix is obtained:

$$\dot{\Psi} = (\nabla f(\mathbf{x_{ob}}) + \mathbf{K}\nabla\mathbf{C}(\mathbf{x_{ob}})(\exp(-\mathbf{H}_\mu\tau) - \mathbb{I}))\Psi \tag{A.7}$$

Finally, the Floquet exponents are extracted by the diagonalization of the fundamental matrix after one period of evolution. In other words they are the solution for the equation:

$$(\Psi(\tau) - \exp(-\mu_n\tau)\mathbb{I}) \cdot \mathbf{v}_\mu = \mathbf{0} \tag{A.8}$$

where $\mathbf{v}_\mu$ are the eigenvectors of $\Psi(\tau)$.

It is important to highlight two important points in this method for the calculation of Floquet exponents. The first is that by introducing delayed states the control actually introduces an infinite number of Floquet exponents to the system, however, the dimension of Eq. (A.7) is the dimension of the system N without the control. This is achieved by using Eq. (A.6) which maintains the dimension of the system. The second point is that the introduction of Eq. (A.6) also makes the fundamental matrix evolution be dependent on the Floquet exponents themselves, $\Psi(\tau) = \Psi(\tau, \mu_n)$. As a consequence of this dependency Eq. (A.8) becomes transcendental with an infinite amount of solutions on the complex plane, in fact, if there is a solution of the type

$\mu_n = \mu_{re} + i\mu_{im}$ then $\mu_{n+j} = \mu_{re} + i[\mu_{im} + 2j\pi]$, for $j \in \mathbb{Z}$, is also a solution.

An optimization method can be used to solve Eq. (A.8). One easy way is to initially have a set of guessed Floquet exponents $\mu_{\mathbf{guess}}$, perform the calculation of the fundamental matrix $\Psi(\tau, \mu_{\mathbf{guess}})$ and afterwards calculate updated Floquet exponents $\mu_{\mathbf{new}}$. hence, one can obtain the Floquet exponents by the minimization of a cost function defined as:

$$d = |\mu_{\mathbf{new}} - \mu_{\mathbf{guess}}| \tag{A.9}$$

where $|\cdot|$ is the Euclidean norm. Finally, any optimization method can be used to bring Eq. (A.9) to its minimum value.

It is important to mention that if the base of solutions is used in the calculation of Floquet exponents then $\mathbf{H}_\mu$ becomes a diagonal matrix which facilitates the optimization and numerical procedure. Another important detail is that one can use the system FE without the ETDF as an initial guess for the calculation of the controlled FE. An example of FE calculation can be found in [38].

Another way to calculate Floquet exponents is through a system time series. Assume that Eq. (A.2) is valid for the deviation $\delta\mathbf{x}$ near the periodic behaviour to be investigated.

$$\delta\mathbf{x}(t) = \mathrm{Re}\left(\sum_{n=1}^{N} (\delta\mathbf{x}(0) \cdot \mathbf{p_n}(0)) \exp(\mu_n t)\mathbf{p_n}(t)\right) \tag{A.10}$$

If it is also assume that $t \gg 1$, all terms of the sum in Eq. (A.10) that have negative or low FE will be much smaller in comparison to the maximum real-valued FE (μ_{max}) term. This allows for the approximation of Eq. (A.2) as follows:

$$\delta\mathbf{x}(t) \approx \mathrm{Re}\left((\delta\mathbf{x}(0) \cdot \mathbf{p_{max}}(0)) \exp(\mu_{max} t)\mathbf{p_{max}}(t)\right) \tag{A.11}$$

where p_{max} is the periodic function related to μ_{max}. Finally if a time series with a period of τ_s is taken the value of $p_{max}(t)$ becomes constant as it is a periodic function. Hence, the time series becomes:

$$\delta\mathbf{x}(n\tau_s) \approx \alpha_\mathbf{0} \exp\left(\mathrm{Re}(\mu_{max})n\tau_s\right) \cos\left(\mathrm{Im}(\mu_{max})n\tau_s\right) \tag{A.12}$$

where $\alpha_\mathbf{0} = (\delta\mathbf{x}(0) \cdot \mathbf{p_{max}}(0))\mathbf{p_{max}}(0)$.

Eq. (A.12) displays that the Poincaré time series of the displacement around a periodic orbit can be modelled by a damped cosine function which has parameters given by the real and imaginary parts of that orbits maximum real-valued FE μ_{max}. Hence, a function calibrated using an experimental time series can be used to extract an orbit μ_{max}.

References

[1] K. Kuribayashi, K. Tsuchiya, Y. Zhong, D. Tomus, M. Umemoto, T. Ito, M. Sasaki, Selfdeployable origami stent grafts as a biomedical application of Ni-rich TiNi shape memory alloy foil, Mater. Sci. Eng. A 419 (2) (2006) 131–137.

[2] M. Salerno, K. Zhang, A. Menciassi, J.S. Dai, A novel 4-DOF origami grasper with an SMA-actuation system for minimally invasive surgery, IEEE Trans. Robot. 32 (3) (2016) 484–498.

[3] W.O.V. Barbosa, A.S. De Paula, M. Savi, D.J. Inman, Chaos control applied to piezoelectric vibration-based energy harvesting systems, Eur. Phys. J. Spec. Top. 224 (14) (2015) 2787–2801.

[4] Q. Cao, M. Wiercigroch, E. Pavlovskaia, C. Grebogi, J.M.T. Thompson, Archetypal oscillator for smooth and discontinuous dynamics, Phys. Rev. E 74 (4) (2006) 046218.

[5] H. Jiang, A.S.E. Chong, Y. Ueda, M. Wiercigroch, Grazing-induced bifurcations in impact oscillators with elastic and rigid constraints, Int. J. Mech. Sci. 127 (2017) 204–214.

[6] D.G. Bassinello, A.M. Tusset, R.T. Rocha, J.M. Balthazar, Dynamical Analysis and control of a chaotic microelectromechanical resonator model, Shock Vib. 2018 (2018) 1–10.

[7] Y. Liu, W. Lin, J.P. Chavez, R. de Sa, Torsional stick–slip vibrations and multistability in drill-strings, Appl. Math. Model. 76 (2019) 545–557.

[8] M. Wiercigroch, Resonance enhanced drilling: method and apparatus, 0000. patent no.WO2007141550.

[9] E. Pavlovskaia, D.C. Hendry, M. Wiercigroch, Modelling of high frequency vibro-impact drilling, Int. J. Mech. Sci. 91 (2015) 110–119.

[10] M. Wiercigroch, V. Vaziri, M. Kapitaniak, RED: Revolutionary Drilling Technology for Hard Rock Formations, Society of Petroleum Engineers, 2017, http://dx.doi.org/10.2118/184665-MS.

[11] F. Nucera, A.F. Vakakis, D.M. McFarland, L.A. Bergman, G. Kerschen, Targeted energy transfers in vibro-impact oscillators for seismic mitigation, Nonlinear Dynam. 50 (3) (2007) 651–677.

[12] S. Wei, H. Hu, S. He, Modeling and experimental investigation of an impact-driven piezoelectric energy harvester from human motion, Smart Mater. Struct. 22 (10) (2013) 105020.

[13] M. Wiercigroch, A.M. Krivtsov, Frictional chatter in orthogonal metal cutting, Phil. Trans. R. Soc. A 359 (2001) 713–738.

[14] C. Budd, F. Felix, Chattering and related behaviour in impact oscillators, Philos. Trans. R. Soc. Lond. Ser. A 347 (1683) (1994) 365–389.

[15] S.R. Bishop, D. Xu, The use of control to eliminate subharmonic and chaotic impacting motions of a driven beam, J. Sound Vib. 205 (2) (1997) 223–234.

[16] E. Pavlovskaia, M. Wiercigroch, C. Grebogi, Modeling of an impact system with a drift, Phys. Rev. E 64 (5) (2001) 056224.

[17] J. Ing, E. Pavlovskaia, M. Wiercigroch, Dynamics of a nearly symmetrical piecewise linear oscillator close to grazing incidence: Modelling and experimental verification, Nonlinear Dynam. 46 (3) (2006) 225–238.

[18] J. Ing, E. Pavlovskaia, M. Wiercigroch, S. Banerjee, Experimental study of impact oscillator with one-sided elastic constraint, Phil. Trans. R. Soc. A 366 (1866) (2008) 679–705.

[19] S. Banerjee, J. Ing, E. Pavlovskaia, M. Wiercigroch, R.K. Reddy, Invisible grazings and dangerous bifurcations in impacting systems: The problem of narrow-band chaos, Phys. Rev. Lett. E 79 (2009) 037201.

[20] J. Ing, E. Pavlovskaia, M. Wiercigroch, S. Banerjee, Bifurcation analysis of an impact oscillator with a one-sided elastic constraint near grazing, Physica D 239 (6) (2010) 312–321.

[21] M. Wiercigroch, S. Kovacs, S. Zong, D. Costa, V. Vaziri, M. Kapitaniak, E. Pavlovskaia, Versatile mass excited impact oscillator, Nonlinear Dynam. 99 (1) (2020) 323–339.

[22] D.D.A. Costa, V. Vaziri, M. Kapitanial, S. Kovacs, E. Pavlovskaia, M. Wiercigroch, Experimental studies of mass excited impact oscillators, Nonlinear Dynam. (2020) http://dx.doi.org/10.1007/s11071-020-05644-0.

[23] E. Ott, C. Grebogi, J.A. Yorke, Controlling chaos, Phys. Rev. Lett. 64 (11) (1990) 1196–1199.

[24] K. Pyragas, Continuous control of chaos by self-controlling feedback, Phys. Lett. A 170 (1992) 421–428.

[25] J.E.S. Socolar, D.W. Sukow, D.J. Gauthier, Stabilizing unstable periodic orbits in fast dynamical systems, Phys. Rev. E 50 (4) (1994) 3245–3248.

[26] J. Lehnert, P. Hövel, V. Flunkert, P.Y. Guzenko, A.L. Fradkov, E. Schöll, Adaptive tuning of feedback gain in time-delayed feedback control, Chaos 21 (4) (2011) 043111.

[27] A. Selivanov, J. Lehnert, A. Fradkov, E. Schöll, Adaptive time-delayed stabilization of steady states and periodic orbits, Phys. Rev. E 91 (1) (2015) 012906.

[28] V. Pyragas, K. Pyragas, Adaptive modification of the delayed feedback control algorithm with a continuously varying time delay, Phys. Lett. A 375 (44) (2011) 3866–3871.

[29] T. Ushio, Limitation of delayed feedback control in nonlinear discrete-time systems, IEEE Trans. Circuits Syst. I 43 (9) (1996) 815–816.

[30] G.A. Leonov, Pyragas stabilizability via delayed feedback with periodic control gain, Systems Control Lett. 69 (2014) 34–37.

[31] W. Just, T. Bernard, M. Ostheimer, E. Reibold, H. Benner, Mechanism of time-delayed feedback control, Phys. Rev. Lett. 79 (2) (1997) 203–206.

[32] K. Pyragas, Control of chaos via an unstable delayed feedback controller, Phys. Rev. Lett. 86 (11) (2001) 2265–2268.

[33] V. Pyragas, K. Pyragas, Act-and-wait time-delayed feedback control of nonautonomous systems, Phys. Rev. E 94 (1) (2016) 012201.

[34] V. Pyragas, K. Pyragas, Act-and-wait time-delayed feedback control of autonomous systems, Phys. Lett. A 382 (8) (2018) 574–580.

[35] V. Pyragas, K. Pyragas, State-dependent act-and-wait time-delayed feedback control algorithm, Commun. Nonlinear Sci. Numer. Simul. 73 (2019) 338–350.

[36] T. Jüngling, A. Gjurchinovski, V. Urumov, Experimental time-delayed feedback control with variable and distributed delays, Phys. Rev. E 86 (4) (2012) 046213.

[37] A.S. De Paula, M.A. Savi, V. Vahid, E. Pavlovskaia, M. Wiercigroch, Experimental bifurcation control of a parametric pendulum, J. Vib. Control 23 (14) (2017) 2256–2268.

[38] D.D.A. Costa, M.A. Savi, A.S. De Paula, D. Bernardini, Chaos control of a shape memory alloy structure using thermal constrained actuation, Int. J. Non-Linear Mech. 111 (2019) 106–118.

[39] A. Saha, P. Wahi, An analytical study of time-delayed control of friction-induced vibrations in a system with a dynamic friction model, Int. J. Non-Linear Mech. 63 (2014) 60–70.

[40] Y. Ding, L. Zheng, R. Yang, Time-delayed feedback control of improved friction-induced model: application to moving belt of particle supply device, Nonlinear Dynam. 100 (1) (2020) 423–434.
[41] B.B. Ferreira, M.A. Savi, A.S. de Paula, Chaos control applied to cardiac rhythms represented by ECG signals, Phys. Scr. 89 (10) (2014) 105203.
[42] A.M. Tusset, M.A. Ribeiro, W.B. Lenz, R.T. Rocha, J.M. Balthazar, Time delayed feedback control applied in an atomic force microscopy (AFM) model in fractional-order, J. Vib. Eng. Technol. 8 (2) (2020) 327–335.
[43] K. Höhne, H. Shirahama, C. Choe, H. Benner, K. Pyragas, W. Just, Global properties in an experimental realization of time-delayed feedback control with an unstable control loop, Phys. Rev. Lett. 98 (21) (2007) 214102.
[44] G.M. Mahmound, A.A. Arafa, T.M. Abed-Elhameed, E.E. Mahmound, Chaos control of integer and fractional orders of chaotic Burke–Shaw system using time delayed feedback control, Chaos Solitons Fractals 104 (2017) 680–692.
[45] A. Soukkou, B. Abdelkrim, A. Goutas, Generalized fractional-order time-delayed feedback control and synchronization designs for a class of fractional-order chaotic systems, Int. J. Gen. Syst. 47 (7) (2018) 679–713.
[46] A.L. Grimsmo, Time-delayed quantum feedback control, Phys. Rev. Lett. 115 (6) (2015) 060402.
[47] L. Droenner, N.L. Naumann, E. Schöll, A. Knorr, A. Carmele, Quantum Pyragas control: Selective control of individual photon probabilities, Phys. Rev. A 99 (2) (2019) 023840.
[48] Z. Zhang, J.P. Chávez, J. Sieber, Y. Liu, Controlling grazing-induced multistability in a piecewise-smooth impacting system via the time-delayed feedback control, Nonlinear Dynam. (2021) http://dx.doi.org/10.1007/s11071-021-06511-2.
[49] Y. Liu, M. Wiercigroch, J. Ing, E. Pavlovskaia, Intermittent control of coexisting attractors, Phil. Trans. R. Soc. A 371 (1993) (2013) 20120428.
[50] Z. Zhi, J.P. Chavez, J. Sieber, Y, Liu controlling coexisting attractors of a class of non-autonomous dynamical systems, Physica D 431 (2022) 133134.
[51] Z. Hao, D. Wang, M, Wiercigroch nonlinear dynamics of new magneto-mechanical oscillator, Commun. Nonlinear Sci. Numer. Simul. 105 (2022) 106092.
[52] P.D. Lax, M.S. Terrell, Calculus with Applications, Springer New York, United States, 2013.
[53] D. Auerbach, P. Cvitanović, J.P. Eckmann, G. Gunaratne, I. Procaccia, Exploring chaotic motion through periodic orbits, Phys. Rev. Lett. 58 (23) (1987) 2387–2389.
[54] K. Pyragas, Delayed feedback control of chaos, Phil. Trans. R. Soc. A 364 (1846) (2006) 2309–2334.
[55] A.S. Purewall, C.M. Postlethwaite, B. Krauskopf, Effect of delay mismatch in Pyragas feedback control, Phys. Rev. E 90 (5) (2014) 052905.
[56] Y. Li, D. Xu, Chaotification of quasi-zero-stiffness system with time delay control, Nonlinear Dynam. 86 (1) (2016) 353–368.